

# Masses, Lifetimes and Production Rates of $\Xi^-$ and $\Xi^+$ at LEP1

Preliminary

DELPHI Collaboration

**B. Åsman, S.O. Holmgren, T. Moa, P. Niss and C. Walck**

University of Stockholm, Fysikum, Box 6730, Stockholm, Sweden

## Abstract

Direct measurements of the  $\Xi^-$  and  $\Xi^+$  masses, lifetimes, and mass and lifetime differences are presented, together with measurements of the inclusive ( $\Xi^- + \Xi^+$ ) production rates in  $Z \rightarrow q\bar{q}$  and  $Z \rightarrow b\bar{b}$  events and of the position  $\xi^*$  of the maximum of the distribution in  $\xi = -\ln x_p$ , where  $x_p$  is the fractional  $\Xi$  momentum.

# 1 Introduction

This paper presents direct measurements of the masses and the mean lifetimes of  $\Xi^-$  and  $\Xi^+$  and of their mass and lifetime differences, together with a study of  $\Xi^{-\dagger}$  production in  $Z^0$  hadronic decays.

The symmetry in the production of particles and antiparticles in  $Z^0$  decays makes direct measurement of  $\Xi^+$  properties with high precision feasible. Previous measurements of the  $\Xi^+$  mass and mean lifetime suffer from low statistics compared to  $\Xi^-$  measurements, since they came from bubble chamber or hyperon beam experiments with a large asymmetry in the production of  $\Xi^-$  and  $\Xi^+$ . The Particle Data Group [1] lists only  $\sim 80$  events used for measurement of the  $\Xi^+$  mass and 34 for its mean lifetime, compared to  $\sim 2400$  for the  $\Xi^-$  mass and  $\sim 80000$  events for its mean lifetime. The present analysis uses about 2500  $\Xi^-$  and 2300  $\Xi^+$ , with small backgrounds.

A measurement is also presented of the production rate of  $\Xi^-$  in  $Z^0 \rightarrow b\bar{b}$  events, together with an update of the previous DELPHI measurement [2] of the average  $\Xi^-$  production rate in hadronic  $Z$  decays.

## 2 The DELPHI Detector and Event Selection

The DELPHI detector is described elsewhere [3, 4]. The detectors most important for this analysis are the Vertex Detector (VD), the Inner Detector (ID), the Time Projection Chamber (TPC), and the Outer Detector (OD). The VD consists of three concentric layers of silicon strip detectors, located at radii 6 cm, 9 cm and 11 cm. The polar angles covered for particles crossing all three layers are  $43^\circ < \theta < 137^\circ$ , where  $\theta$  is given with respect to the  $z$  axis<sup>†</sup>. In 1994 and 1995, the first and third layers had double-sided readout and gave both  $R\phi$  and  $z$  coordinates. The TPC is the main tracking device where charged particle tracks are reconstructed in three dimensions for radii between 29 cm and 122 cm. The ID and OD are two drift chambers located at radii between 12 cm and 28 cm and between 198 cm and 206 cm respectively, and provide additional points for the track reconstruction.

A charged particle was accepted in the analysis if its track length was above 30 cm, its momentum above 100 MeV/c, and its relative momentum error below 100%.

An event was classified as hadronic if it had at least 7 charged particles with momentum above 200 MeV/c carrying more than 15 GeV total reconstructed energy, and at least 3 GeV in each hemisphere.

The analysis used 3.25 million reconstructed hadronic decays of the  $Z$ , consisting of 0.67 million from the 1992 run, 0.68 million from 1993, 1.29 million from 1994, and 0.61 million from 1995.

Simulated events were produced using the JETSET parton shower generator [5], and then processed with the DELPHI event simulation program DELSIM [6] which fully simulates all detector effects. For each year (1992-1994)  $\sim 1$  million fully simulated  $q\bar{q}$  events were analyzed in the same way as the real data, and about 0.6 million for 1995. The total

---

<sup>†</sup>Antiparticles are implicitly referenced if not explicitly stated otherwise.

<sup>‡</sup>In the standard DELPHI coordinate system, the  $z$  axis is along the electron direction, the  $x$  axis points towards the centre of LEP, and the  $y$  axis points upwards. The polar angle to the  $z$  axis is called  $\theta$  and the azimuthal angle around the  $z$  axis is called  $\phi$ ; the radial coordinate is  $R = \sqrt{x^2 + y^2}$ .

number of simulated events used was thus about 3.6 million, comparable to the number of real events. The number of  $\Xi^-$  and  $\Xi^+$  decays generated in the simulation was about 89000.

### 3 Analysis

The  $\Xi^-$  hyperon was studied by a complete reconstruction of the decay chain  $\Xi^- \rightarrow \Lambda \pi^-$ , where  $\Lambda \rightarrow p \pi^-$ . The same analysis procedure was used previously for  $\Omega^-$  reconstruction [7, 8]. Further details are given in [9].

All pairs of oppositely charged particles were tried in a search for  $\Lambda$  candidates. For each such pair, a vertex fit was performed by the standard DELPHI  $V^0$  search algorithm<sup>§</sup>. A pair was accepted as a  $\Lambda$  candidate if the  $\chi^2$ -probability of the secondary vertex fit exceeded 0.1%, the measured flight distance of the  $\Lambda$  candidate in the  $xy$  plane exceeded twice its error, and the angle between the momentum vector sum of the two tracks and the vector joining the primary and secondary vertices was less than 0.1 rad. The inclusive  $\Lambda$  reconstruction efficiency was around 19% [4], including the 63.9% branching ratio of  $\Lambda \rightarrow p \pi^-$  [1]. The invariant mass of the  $\Lambda$  candidate was required to be between 1.105 GeV/c<sup>2</sup> and 1.125 GeV/c<sup>2</sup>.

One by one, the remaining charged particles that crossed the  $\Lambda$  trajectory in the  $xy$  plane were then combined with the  $\Lambda$  candidate to form a  $\Xi^-$  candidate. All  $\Xi^-$  were assumed to originate from the beam interaction point, which was calculated event by event.

A constrained fit was performed if

- the intersection between the  $\Lambda$  and the charged particle trajectories was more than 8 mm away from the main vertex in the  $xy$  plane,
- the  $\Lambda$  and charged particle trajectories were less than 7 mm apart in the  $z$  direction at the point of crossing in the  $xy$  plane,
- and the charged particle had an impact parameter with respect to the main vertex in the  $xy$  plane of at least 0.5 mm.

The fit used was a general least squares fit with kinematical and geometrical constraints applied to each  $\Xi^-$  candidate. The 16 measured variables in the fit were the five parameters of the helix parameterization of each of the three charged particle tracks and the  $z$  coordinate of the beam interaction point; the  $x$  and  $y$  coordinates were so precisely measured that they were taken as fixed. The two unmeasured variables were the decay radii of the  $\Xi^-$  and  $\Lambda$ . The  $\Xi^-$  decay point was then determined from this  $\Xi^-$  decay radius and the  $\pi^-$  trajectory while the  $\Lambda$  decay point was determined from the point on the proton trajectory at the  $\Lambda$  decay radius. The curved  $\Xi^-$  track was not measured, but calculated in the fit.

Four constraints required the momenta of the  $\Xi^-$  and  $\Lambda$  at their decay points to be in the same direction as the trajectory joining their production and decay positions, two

---

<sup>§</sup>A  $V^0$  consists of two oppositely charged particles originating from a neutral particle decaying in flight.

required the other  $\pi^-$  to meet the proton at the  $\Lambda$  decay radius, and the last (seventh) constrained the  $\Lambda$  mass to its nominal value<sup>¶</sup>.

The pull distributions of the 16 fitted quantities were all approximately normally distributed, with mean 0 within  $\pm 0.1$  and standard deviation 1 within  $\pm 0.1$ , both for data and for the simulated events.

The following cuts were used to select the  $\Xi^-$  and  $\Xi^+$  samples:

- the  $\chi^2$ -probability of the fit had to exceed 1%;
- the  $\Xi$  momentum had to fulfill  $1.2 < \xi < 4.2$  where  $\xi = -\ln x_p$  and  $x_p = p_{\Xi^-}/p_{beam}$ , which corresponds approximately to  $0.015 < x_p < 0.3$  or  $\Xi$  momentum between 0.7 and 14 GeV/c<sup>2</sup>;
- the  $\Xi$  momentum had to point into the barrel region of the detector ( $|\cos \theta| < 0.85$ );
- the decay radius of the  $\Xi$  in the  $xy$  plane had to exceed 2 cm;
- the decay radius of the  $\Xi$  in the  $xy$  plane had to be less than the  $\Lambda$  decay radius.

The agreement between data and simulation was very good. Figure 1 shows the  $\Xi$  signals before and after the cuts were applied. The distributions of the variables used in the selection of  $\Xi$  candidates are compared in Figure 2.

The fit gave a narrow mass peak from  $\Xi^-$  decays on a small background, as shown in Figure 3a;  $2474 \pm 62$   $\Xi^-$  and  $2265 \pm 60$   $\Xi^+$  decays were reconstructed, as shown in Figures. 3b and 3c. The fitted curves consist of a linear term for the background, and two Gaussian distributions with common mean for the signal. The fitted widths of the two Gaussians were  $(2.0 \pm 0.1)$  MeV/c<sup>2</sup> and  $(5.6 \pm 0.4)$  MeV/c<sup>2</sup>, with a relative fraction of  $1.31 \pm 0.15$ . The corresponding widths from fitting simulated data were  $(1.8 \pm 0.1)$  MeV/c<sup>2</sup> and  $(5.6 \pm 0.5)$  MeV/c<sup>2</sup>, with a relative fraction of  $2.11 \pm 0.21$ . This parameterization of signal and background was used in the determination of the  $\Xi^-$  and  $\Xi^+$  masses.

### 3.1 Measurement of $\Xi^-$ and $\Xi^+$ masses and mass difference

In order to determine the masses of the  $\Xi^-$  and  $\Xi^+$ , fully simulated events were used to investigate possible mass shifts. The  $\Xi$  mass in the simulation was set to 1321.3 MeV/c<sup>2</sup>. Table 1 gives the fitted mass values for both the real and simulated data. As already described, the signal (see Figure 3) was represented by two Gaussian distributions with common mean and the background by a linear term.

In order to correct for any bias due to the fit procedure, the mass values obtained from the data were corrected by the difference between the value obtained from the simulated events and the input value used in the simulation. The average correction amounted to  $-0.07 \pm 0.04$  MeV/c<sup>2</sup>.

Further systematic uncertainties could arise from errors in the magnetic field or errors in applying the dE/dX corrections to the particle momenta due to uncertainties in the material description.

Changing the assumed magnetic field value by 0.2% was found to change the mean fitted  $\Xi$  mass by about 0.20 MeV/c<sup>2</sup>. Since 1992, the magnetic field has been monitored

---

<sup>¶</sup>The nominal  $\Lambda$  mass was taken to be  $1115.684 \pm 0.006$  MeV/c<sup>2</sup> [1].

Year	92	93	94	95
$M_{\Xi^-} - 1321.3$ in MC	$0.07 \pm 0.10$	$-0.01 \pm 0.09$	$0.06 \pm 0.11$	$0.18 \pm 0.12$
$M_{\Xi^-} - 1321.3$ in data	$0.70 \pm 0.17$	$0.24 \pm 0.15$	$0.35 \pm 0.10$	$0.45 \pm 0.16$
Corrected $M_{\Xi^-}$ :	$1321.93 \pm 0.20$	$1321.55 \pm 0.17$	$1321.59 \pm 0.15$	$1321.57 \pm 0.20$
$M_{\Xi^+} - 1321.3$ in MC	$0.17 \pm 0.11$	$-0.06 \pm 0.10$	$0.04 \pm 0.12$	$0.31 \pm 0.14$
$M_{\Xi^+} - 1321.3$ in data	$0.61 \pm 0.17$	$0.30 \pm 0.15$	$0.40 \pm 0.12$	$-0.06 \pm 0.18$
Corrected $M_{\Xi^+}$ :	$1321.74 \pm 0.20$	$1321.66 \pm 0.18$	$1321.66 \pm 0.17$	$1320.93 \pm 0.23$
$M_{\Xi^\pm} - 1321.3$ in MC	$0.13 \pm 0.07$	$-0.02 \pm 0.07$	$0.03 \pm 0.08$	$0.25 \pm 0.09$
$M_{\Xi^\pm} - 1321.3$ in data	$0.58 \pm 0.12$	$0.30 \pm 0.10$	$0.39 \pm 0.08$	$0.28 \pm 0.12$
Corrected $M_{\Xi^\pm}$ :	$1321.75 \pm 0.14$	$1321.62 \pm 0.12$	$1321.66 \pm 0.11$	$1321.33 \pm 0.15$
$M_{\Xi^-} - M_{\Xi^+}$ in data	$0.09 \pm 0.24$	$-0.06 \pm 0.21$	$-0.05 \pm 0.16$	$0.51 \pm 0.24$
$M_{\Xi^-} - M_{\Xi^+}$ in MC	$-0.10 \pm 0.15$	$0.05 \pm 0.13$	$0.02 \pm 0.16$	$-0.13 \pm 0.18$

Table 1:  $\Xi^-$  and  $\Xi^+$  mass fit results. Values are in MeV/c<sup>2</sup>. In the simulated sample, the generated  $\Xi^-$  mass was 1321.3 MeV/c. The errors are statistical only.

from time to time by 5 NMR probes located at fixed positions around the TPC. Pending detailed study of these data, a conservative error of  $\pm 0.30\%$  is currently assigned, corresponding to a mass uncertainty  $\pm 0.30$  MeV/c<sup>2</sup>.

On average the dE/dx correction added about 7 MeV to the energy of the pion from the  $\Xi$  decay. The fitted masses were found not to depend on the momentum of this pion, which is generally the decay product passing through the most material and is not affected by the  $\Lambda$  mass constraint, and is thus the one most sensitive to dE/dX corrections. The combined  $\Xi^-$  and  $\Xi^+$  data sample was divided into 9 pion momentum bins, each with a width of 100 MeV/c, starting at 100 MeV/c. In each bin, the  $\Xi$  mass was fitted. No systematic effect depending on the pion momentum was observed. As shown in Table 2 the  $\Xi$  mass was also measured as a function of the polar angle of the  $\Xi$  momentum and of the observed distance in the  $xy$  plane from the beam axis. No significant variation was found. Changing the dE/dX correction by  $\pm 20\%$  changed the mean fitted  $\Xi$  mass by  $\pm 0.05$  MeV/c<sup>2</sup>. This amount was also considered as a systematic error contribution.

The  $\Xi$  mass values observed in the different years were only marginally consistent, with a  $\chi^2$  probability of 8%. The data from different years were therefore treated as

$ \cos(\Theta) $	0.00 – 0.20	0.20 – 0.50	0.50 – 0.85	—
Corrected $M_{\Xi^\pm}$	$1321.44 \pm 0.14$	$1321.64 \pm 0.09$	$1321.57 \pm 0.11$	—
$d_{xy}$ (cm)	0 – 5	5 – 10	10 – 20	> 20
Corrected $M_{\Xi^\pm}$	$1321.69 \pm 0.09$	$1321.49 \pm 0.11$	$1321.54 \pm 0.15$	$1321.47 \pm 0.22$

Table 2: Corrected  $\Xi^\pm$  mass values as functions of  $|\cos(\Theta)|$ , where  $\Theta$  is the angle between the  $\Xi$  momentum and the beam axis, and the decay distance  $d_{xy}$  of the  $\Xi$  in the plane perpendicular to the beam axis. The errors are statistical only.

different experiments, applying the PDG error-scaling procedure to their combination <sup>||</sup> and treating the added error as an additional systematic error. This led to a further contribution of  $\pm 0.07$  MeV/ $c^2$ .

As a further check of the procedure, the Monte Carlo correction method used above was also used to determine the  $\Lambda$  mass. The  $\Lambda$  sample was the same as the one used for the  $\Xi^-$  and  $\Xi^+$  reconstruction. The  $\Lambda$  decays were reconstructed by considering all pairs of oppositely charged particles, and the vertex defined by each pair was determined by minimizing the  $\chi^2$  of the extrapolated tracks. Consequently, in this case the fit procedure was different, and the Monte Carlo correction was found to be essential. It was much larger and of the opposite sign,  $+0.61 \pm 0.01$  MeV/ $c^2$ . Taking the weighted average of the results for the four years, the  $\Lambda$  mass was found to be  $1115.57 \pm 0.02$  MeV/ $c^2$ . This is  $0.12 \pm 0.02$  MeV/ $c^2$  below the nominal value. Corresponding systematic errors on the  $\Xi$  mass scale of  $\pm 0.12$  MeV/ $c^2$  and  $\pm 0.02$  MeV/ $c^2$  were considered. The systematic error contributions are summarized in Table 3.

Thus the average  $\Xi$  masses found are:

$$\begin{aligned}
M_{\Xi^-} &= 1321.63 \pm 0.09 \text{ (stat.)} \pm 0.33 \text{ (syst.) MeV}/c^2 \\
M_{\Xi^+} &= 1321.55 \pm 0.09 \text{ (stat.)} \pm 0.33 \text{ (syst.) MeV}/c^2 \\
M_{\Xi^-+\Xi^+} &= 1321.61 \pm 0.06 \text{ (stat.)} \pm 0.33 \text{ (syst.) MeV}/c^2,
\end{aligned}$$

where the systematic errors quoted are common to all three values.

The systematic errors cancel in the mass difference, where the small statistical errors on the uncorrected values can be fully exploited. The mass difference measured in data is

---

<sup>||</sup>A procedure for averaging data from different experiments is discussed in [1]. If data from  $N$  different experiments are to be combined, then they are usually weighted by  $w_i = 1/\sigma_i^2$ , where  $\sigma_i$  is the combined statistical and systematic error of the  $i$ :th experiment added in quadrature. If the

$$\chi^2 = \sum_i^N w_i (\bar{x} - x_i)^2$$

of the average is too poor then the experiments do not agree. In this case, and if no experiment(s) can be singled out as erroneous, then they should all be treated in the same way. All errors are then scaled with a factor  $S = \sqrt{\chi^2/N_{dof}}$ , where  $N_{dof} = N - 1$  is the expectation value for a chi-squared variable with  $N - 1$  degrees of freedom. When the quoted combined statistical and systematic errors are not sufficient to account for observed discrepancies between the experiments, this procedure can be used to find the systematic that 'explains' the observed spread. Starting from the statistical error  $e_{stat}$  and the factor  $S$ , the scaled error  $S e_{stat}$  can be decomposed into the original statistical error  $e_{stat}$  and a systematic component  $e_{syst} = \sqrt{(S^2 - 1)} e_{stat}$ .

Source	MeV/c <sup>2</sup>
magnetic field uncertainty	±0.30
dE/dX uncertainty	±0.05
year-by-year variation	±0.07
Λ mass shift	±0.12
Λ mass shift uncertainty	±0.02
total	±0.33

Table 3: Systematic error contributions to the  $\Xi$  mass measurement.

$$\Delta_M = M_{\Xi^-} - M_{\Xi^+} = 0.06 \pm 0.10 \text{ MeV}/c^2$$

which corresponds to a fractional mass difference of

$$(M_{\Xi^-} - M_{\Xi^+})/M_{average} = (4.8 \pm 7.7) \times 10^{-5}.$$

### 3.2 Measurement of $\Xi^-$ and $\Xi^+$ lifetimes and lifetime difference

The measurement of the mean lifetimes of the  $\Xi^-$  and  $\Xi^+$  uses the  $\Xi^-$  and  $\Xi^+$  candidates with a  $\Lambda\pi$  invariant mass within  $\pm 5 \text{ MeV}/c^2$  of the nominal mass, where the signal to background ratio was about 6:1. This is the sample for which data and simulation were compared in detail in Figure 2. The mean lifetimes were estimated using a maximum likelihood fit. The time distribution of the combinatorial background was estimated simultaneously in the fit by using the wrong sign combinations. The observed proper time distributions and the fitted functions for the right sign and wrong sign distributions are shown in Figures. 4 and 5 respectively. As the mean lifetimes of  $c$ - and  $b$ -baryons are much shorter than for  $\Xi$ , all  $\Xi$  may safely be assumed to originate from the interaction point.

The proper time was calculated as

$$t = d_{\Xi} M_{\Xi} / P_{\Xi} \quad (1)$$

where  $d_{\Xi}$  is the fitted flight distance,  $P_{\Xi}$  is the fitted momentum of the  $\Xi$  candidate in the  $xy$  plane and  $M_{\Xi}$  is the nominal  $\Xi$  mass.

For right and wrong sign candidates in the proper time interval 0.04 ns to 2.0 ns, the following likelihood function was formed:

$$\mathcal{L} = \prod_{i=1}^{N_{rs}} F(t_i) \cdot \prod_{j=1}^{N_{ws}} B(t_j). \quad (2)$$

The first factor, the  $F(t)$  product, represents the right sign ( $\Lambda\pi^-$ ,  $\bar{\Lambda}\pi^+$ ) combinations. The second factor, the  $B(t)$  product, is an empirical parameterization of the wrong sign ( $\Lambda\pi^+$ ,  $\bar{\Lambda}\pi^-$ ) combinations. The same function  $B(t)$  was also used to describe the background in the right-sign sample. Thus, by maximizing the joint likelihood function  $\mathcal{L}$ , the background contribution in the right sign sample was naturally constrained to the shape of the wrong sign distribution.

The right-sign function  $F(t)$  was given by

$$F(t) = \frac{1}{\sigma_0 + 1} (\sigma_0 S(t) + B(t)) \quad (3)$$

where  $S(t)$  is a normalized probability density function for the observed signal, *i.e.* it is proportional to  $\epsilon(t)e^{-t/\tau_\Xi}$ , where  $\epsilon(t)$  is an empirical efficiency parameterization of the time-dependent form  $e^{(c_1+c_2t)}$ . The relative normalization of the signal  $S(t)$  and background  $B(t)$  in the right-sign sample,  $\sigma_0$ , was fixed by the observed number of right sign ( $N_{rs}$ ) and wrong sign ( $N_{ws}$ ) events in the fitted time interval 0.04 ns to 2.0 ns,  $\sigma_0 = \frac{N_{rs}-N_{ws}}{N_{ws}}$ .

The background function  $B(t)$  was given by

$$B(t) = \frac{1}{b_1 + 1} \left\{ b_1 \frac{b(t; \sigma_1)}{\mathcal{N}_1} + \frac{b(t; \sigma_2)}{\mathcal{N}_2} \right\} \quad (4)$$

where

$$b(t; \sigma_i) = \frac{1}{\Gamma(\beta)\sigma_i} \left( \frac{t}{\sigma_i} \right)^{\beta-1} e^{-\frac{t}{\sigma_i}}. \quad (5)$$

and  $\mathcal{N}_1$  and  $\mathcal{N}_2$  are normalization constants for the two  $\Gamma$ -distributions  $b(t; \sigma_i)$ . We found that  $\beta = 3$  provides a good description of the wrong sign distribution. The parameters  $b_1$ ,  $\sigma_1$  and  $\sigma_2$  were fitted to the data, together with  $\tau_\Xi$ .

The measured  $\Xi^-$  and  $\Xi^+$  lifetimes are:

$$\begin{aligned} \tau_{\Xi^-} &= 0.165 \pm 0.007 \text{ (stat.)} \pm 0.012 \text{ (syst.) ns} \\ \tau_{\Xi^+} &= 0.170 \pm 0.008 \text{ (stat.)} \pm 0.012 \text{ (syst.) ns} \\ \tau_{\Xi^-+\Xi^+} &= 0.167 \pm 0.006 \text{ (stat.)} \pm 0.012 \text{ (syst.) ns} \end{aligned}$$

where the results were achieved by performing the same analysis on the four separate years. The lifetimes were taken as the weighted average of the four years.

In order to minimize the effect of statistical fluctuations, the combined  $\Xi^-$  and  $\Xi^+$  sample was used to evaluate the systematic errors. The following sources of systematic errors were considered:

- The effect on the lifetime fits due to the uncertainty in the parameters  $c_1$  and  $c_2$  in the efficiency parameterization were estimated by a Monte Carlo procedure. The contributions were found to be of the order of  $\pm 0.005$  ns.
- The difference between the simulated and reconstructed lifetimes in the simulation was  $0.002 \pm 0.004$  ns.
- Changing the fit range in proper time typically changed the fitted lifetime by  $\pm 0.004$  ns.
- Changing the value of  $\beta$  (Equation. 5) in the range 1.5 to 4.0 did not produce any significant influence on the final results.
- The  $\chi^2$  of the combination of the four different years was 14.1 for 3 degrees of freedom. This corresponds to a probability of only 0.3%. Applying the PDG scaling procedure to the combination gives an additional systematic error of  $\pm 0.011$  ns.



Further discussions on the evaluation of the systematic errors may be found in [9].

Note that a  $\Xi$  could be reconstructed only if the (anti)proton from the (anti)lambda was seen in the TPC. Therefore the fact that more antibaryons than baryons interacted in the material before the TPC reduced the relative number of  $\Xi^+$  reconstructed by about 10%, but had little effect on their lifetime distribution. As the systematic errors cancel in the measurement of the lifetime difference:

$$\Delta\tau = \tau_{\Xi^-} - \tau_{\Xi^+} = -0.004 \pm 0.011 \text{ ns}$$

which gives a fractional lifetime difference of

$$(\tau_{\Xi^-} - \tau_{\Xi^+})/\tau_{average} = -0.03 \pm 0.07,$$

and the value of  $\Delta\tau$  may be used together with the world average for the  $\Xi^-$  lifetime,  $\tau_{\Xi^-}^{PDG} = 0.1639 \pm 0.0015 \text{ ns}$ , to make a new precise determination of the  $\Xi^+$  lifetime alone:

$$\tau_{\Xi^+} = \tau_{\Xi^-}^{PDG} - \Delta\tau = 0.17 \pm 0.01 \text{ ns}$$

### 3.3 Measurement of $\Xi^-$ and $\Xi^+$ Production

The parameterization of the signal used in the  $\Xi$  mass determination was not used to evaluate the efficiencies and production rates, since the broader Gaussian tended to become unreasonably wide if left free when fitting smaller data samples. Instead, as in the lifetime analysis just described, the interval of  $\pm 5 \text{ MeV}/c^2$  around the nominal  $\Xi^-$  mass was used as signal region, and the background was estimated from the wrong sign ( $\Lambda\pi^+$  and  $\bar{\Lambda}\pi^-$ ) invariant mass distributions. The effect of varying the width of the signal region was very small.

The efficiency depended on the  $\Xi$  momentum (see Table 4 and Figure 6). The average efficiency was found to be  $(6.33 \pm 0.26 \text{ (stat.)}) \%$  for the combined  $\Xi^-$  and  $\Xi^+$  reconstruction, including cuts and the 63.9 % branching ratio for  $\Lambda \rightarrow p\pi^-$ . The error comes from the finite number of simulated events. As mentioned earlier, the reconstruction efficiency was  $\sim 10 \%$  lower for  $\Xi^+$  than for  $\Xi^-$ , due to differences in the cross sections for hadronic interactions of particles and antiparticles in the detector material.

All  $\Xi^-$  candidates satisfying the standard  $\Xi^-$  cuts, and with an  $\Lambda\pi^-$  invariant mass within  $\pm 5 \text{ MeV}/c^2$  of the nominal  $\Xi^-$  mass, were considered. The background contribution was estimated from the wrong sign combinations and was subtracted. The measured distribution in  $\xi = -\ln x_p$  is shown in Figure 6 and Table 4. The  $< \Xi^- + \Xi^+ >$  production rate in the  $\xi$  interval  $1.4 < \xi < 4.0$  was found to be

$$< \Xi^- + \Xi^+ >_{q\bar{q}} = 0.0187 \pm 0.0007 \text{ (stat.)}$$

where the statistical error includes the contributions from data and simulation. Extrapolating to the full momentum range using the JETSET prediction gave

$$< \Xi^- + \Xi^+ >_{q\bar{q}} = 0.0233 \pm 0.0007 \text{ (stat.)} \pm 0.0024 \text{ (syst.)}$$

in hadronic  $Z$  decays. This result agrees with the previously published value of  $0.0250 \pm 0.0009 \pm 0.0021$  [2], obtained using a somewhat different  $\Xi$  reconstruction procedure. The DELPHI tuned JETSET 7.3 [10] gives  $< \Xi^- + \Xi^+ >_{q\bar{q}} = 0.0251$  and JETSET 7.4 with default parameters gives 0.0273, whereas HERWIG 5.9 gives  $< \Xi^- + \Xi^+ >_{q\bar{q}} = 0.0730$ .

Momentum (GeV/c)	$x_p$	$\xi = -\ln x_p$	Efficiency (%)	Reconstructed $\Xi^-$	$N_{\Xi}/\text{bin/event}$
11.24–13.73	0.246–0.301	1.2–1.4	—	—	—
9.21–11.24	0.202–0.246	1.4–1.6	$1.6 \pm 0.4$	$58 \pm 16$	$0.00112 \pm 0.00041$
7.54–9.21	0.165–0.202	1.6–1.8	$3.5 \pm 0.4$	$154 \pm 20$	$0.00137 \pm 0.00025$
6.17–7.54	0.135–0.165	1.8–2.0	$4.7 \pm 0.4$	$257 \pm 26$	$0.00169 \pm 0.00023$
5.05–6.17	0.111–0.135	2.0–2.2	$7.7 \pm 0.5$	$421 \pm 31$	$0.00168 \pm 0.00016$
4.14–5.05	0.091–0.111	2.2–2.4	$9.8 \pm 0.6$	$541 \pm 33$	$0.00171 \pm 0.00014$
3.39–4.14	0.074–0.091	2.4–2.6	$11.1 \pm 0.6$	$673 \pm 35$	$0.00186 \pm 0.00014$
2.77–3.39	0.061–0.074	2.6–2.8	$11.0 \pm 0.6$	$714 \pm 36$	$0.00199 \pm 0.00014$
2.27–2.77	0.050–0.061	2.8–3.0	$12.2 \pm 0.6$	$663 \pm 34$	$0.00167 \pm 0.00011$
1.86–2.27	0.041–0.050	3.0–3.2	$11.1 \pm 0.6$	$562 \pm 29$	$0.00156 \pm 0.00011$
1.52–1.86	0.033–0.041	3.2–3.4	$8.3 \pm 0.5$	$384 \pm 25$	$0.00143 \pm 0.00012$
1.25–1.52	0.027–0.033	3.4–3.6	$6.3 \pm 0.5$	$196 \pm 19$	$0.00096 \pm 0.00012$
1.02–1.25	0.022–0.027	3.6–3.8	$4.2 \pm 0.4$	$118 \pm 15$	$0.00087 \pm 0.00014$
0.84–1.02	0.018–0.022	3.8–4.0	$2.3 \pm 0.4$	$57 \pm 11$	$0.00077 \pm 0.00020$
0.68–0.84	0.015–0.018	4.0–4.2	—	—	—

Table 4:  $\Xi^-$  efficiency and  $\xi$  distribution. The extreme points have been omitted because of their large errors.

The quoted systematic error has the following two sources. According to the simulation, 20% of the  $\Xi^-$  and  $\Xi^+$  were produced outside the range  $1.4 < \xi < 4.0$ . An error of 50% of this number was taken as a contribution to the total systematic error. Secondly, adding a cut on lifetime,  $\tau_{\Xi} > 0.1$  ns, and requiring the  $\Lambda$  candidate to be tagged as a 'tight'  $\Lambda$  ( $xy$  flight distance above four standard deviations and  $\chi^2$  probability larger than 1 %) by the  $V^0$  reconstruction program gives a very clean sample. The production rate calculated with this sample is  $0.0243 \pm 0.0012(\text{stat.})$ , which is the same as those above within errors. The half-difference of the rates calculated with the two different sets of cuts was added in quadrature to give the total systematic error.

From a Gaussian fit, the  $\xi$  distribution was found to have a maximum at

$$\xi_{data}^* = 2.56 \pm 0.05 (\text{stat.}) \pm 0.03 (\text{syst.}) .$$

The systematic error quoted is the half-difference of the  $\xi^*$  values found using the 'standard' and 'tight' cuts. The JETSET model, with parameters tuned as in [10], gives  $\xi_{JETSET}^* = 2.506 \pm 0.004(\text{stat.})$  from a fit to a modified Gaussian form [11].

The large statistics of the generated  $\Xi^-$  sample clearly showed that the generated  $\xi$  distribution was not Gaussian. However, fitting a Gaussian distribution to the generated  $\xi$  spectrum gave  $\xi^* = 2.522 \pm 0.004$ , very close to the result of fitting the modified Gaussian. Fitting the modified form to real data, and keeping the skewness and kurtosis parameters fixed to the values found in the simulation, gave  $\xi^* = 2.51 \pm 0.06(\text{stat.})$ .

The above procedure for finding  $\Xi^-$  was also applied to  $Z \rightarrow b\bar{b}$  decays. The  $b\bar{b}$  events were selected with a lifetime tag algorithm, originally developed by the ALEPH Collaboration [12] and later adapted for DELPHI data [13]. This technique is based on the measurement of the impact parameter of each particle relative to the  $Z^0$  production point. Decay products from particles with relatively long lifetimes, like B-hadrons, will have large impact parameters. Particles produced in the primary interaction will have impact parameters with a spread around zero according to the spatial resolution of the detector. From all tracks with a positive impact parameter in an event, a probability for the hypothesis that they all came from a single point was calculated. Events in which this probability was below 1% were selected as  $b\bar{b}$  events. The joint efficiency to reconstruct a  $\Xi^-$  decay and simultaneously tag a  $b\bar{b}$  event with this cut was about 3%, with a  $b\bar{b}$  purity of 77%.

Taking the weighted average of the results from the four years gives the following production rate of  $\Xi^-$  and  $\Xi^+$  in  $b\bar{b}$  events:

$$\langle \Xi^- + \Xi^+ \rangle_{b\bar{b}} = 0.0183 \pm 0.0016 \text{ (stat.)} \pm 0.0035 \text{ (syst.)}$$

where the systematic error comes from the momentum extrapolation and the sample variation of the four years data. Different cuts on the probability as well as looser  $\Xi^-$  selections have been tested. The value of  $\langle \Xi^- + \Xi^+ \rangle_{b\bar{b}}$  changed only within  $\pm 0.001$ . The DELPHI tuned JETSET 7.3 [10] gives  $\langle \Xi^- + \Xi^+ \rangle_{b\bar{b}} = 0.0238$  and JETSET 7.4 with default parameters gives 0.0208, whereas HERWIG 5.9 gives  $\langle \Xi^- + \Xi^+ \rangle_{b\bar{b}} = 0.0523$ .

## 4 Summary

About 2500  $\Xi^-$  and 2300  $\Xi^+$  decays have been reconstructed.

From this large sample, direct measurements have been made of the  $\Xi^-$  and  $\Xi^+$  masses and their average and difference:

$$\begin{aligned} M_{\Xi^-} &= 1321.63 \pm 0.09 \text{ (stat.)} \pm 0.33 \text{ (syst.) MeV}/c^2 \\ M_{\Xi^+} &= 1321.55 \pm 0.09 \text{ (stat.)} \pm 0.33 \text{ (syst.) MeV}/c^2 \\ M_{\Xi^- + \Xi^+} &= 1321.61 \pm 0.06 \text{ (stat.)} \pm 0.33 \text{ (syst.) MeV}/c^2 \\ M_{\Xi^-} - M_{\Xi^+} &= 0.06 \pm 0.10 \text{ MeV}/c^2 \\ (M_{\Xi^-} - M_{\Xi^+})/M_{average} &= (4.8 \pm 7.7) \times 10^{-5}, \end{aligned}$$

The masses given by the PDG [1] are  $M_{\Xi^-} = 1321.34 \pm 0.14 \text{ MeV}/c^2$ ,  $M_{\Xi^+} = 1321.20 \pm 0.33 \text{ MeV}/c^2$  and  $(M_{\Xi^-} - M_{\Xi^+})/M_{average} = (11 \pm 27) \times 10^{-5}$ . Up to now only small samples of  $\Xi^+$  are referenced by the PDG [1].

The  $\Xi^-$  lifetime measurement obtained is consistent with the PDG value, but the PDG value is more precise. For the lifetime difference we obtain

$$\Delta\tau = \tau_{\Xi^-} - \tau_{\Xi^+} = -0.004 \pm 0.011 \text{ ns}$$

implying

$$\begin{aligned} (\tau_{\Xi^-} - \tau_{\Xi^+})/\tau_{average} &= -0.03 \pm 0.07 \\ \tau_{\Xi^+} &= 0.17 \pm 0.01 \text{ ns}, \end{aligned}$$

where the  $\tau_{\Xi^+}$  value uses the PDG value [1] for the  $\Xi^-$  lifetime,  $\tau_{\Xi^-} = 0.1639 \pm 0.0015$  ns. The PDG value [1] for the  $\Xi^+$  lifetime is  $\tau_{\Xi^+} = 0.16 \pm 0.03$  ns. For the fractional lifetime difference, PDG quote  $(\tau_{\Xi^-} - \tau_{\Xi^+})/\tau_{average} = 0.02 \pm 0.18$ .

The inclusive production rates for  $\Xi^-$  plus  $\Xi^+$  in hadronic Z decays and in  $Z \rightarrow b\bar{b}$  decays were found to be:

$$\begin{aligned} \langle \Xi^- + \Xi^+ \rangle_{q\bar{q}} &= 0.0233 \pm 0.0007 (stat.) \pm 0.0024 (syst.) \\ \langle \Xi^- + \Xi^+ \rangle_{b\bar{b}} &= 0.0183 \pm 0.0016 (stat.) \pm 0.0030 (syst.) \end{aligned}$$

The predictions by JETSET are in agreement with these measurements, whereas the predictions by HERWIG are not. The maximum of the variable  $\xi = -\ln x_p$  was found to be at

$$\xi^* = 2.56 \pm 0.05 (stat.) \pm 0.03 (syst.)$$

in hadronic Z decays. Other LEP experiments have reported similar results on  $\Xi^-$  production in  $Z^0$  decays [14, 15].

These results are preliminary. In particular, it is hoped that the systematic error on the mass measurements can be substantially reduced when the analysis is completed.

## Acknowledgements

We are greatly indebted to our technical collaborators and to the funding agencies for their support in building and operating the DELPHI detector, and to the members of the CERN-SL Division for the excellent performance of the LEP collider.

## References

- [1] Particle Data Group, Phys. Rev. **D50** (1994) 1173.
- [2] DELPHI Collaboration, P. Abreu et al., Z.Phys. **C67** (1995) 543.
- [3] DELPHI Collaboration, P. Aarnio et al., Nucl. Instr. and Meth. **A303** (1991) 233.
- [4] DELPHI Collaboration, P. Abreu et al., Nucl. Instr. and Meth. **A378** (1996) 57.
- [5] T. Sjöstrand, Comput. Phys. Commun. **82** (1994) 74-89.
- [6] DELSIM User's Guide, DELPHI 89-15 PROG 130, CERN, February 1989  
DELSIM Reference Manual, DELPHI 89-68 PROG 143, CERN, September 1989.
- [7] "Production of  $\Xi^-$  and  $\Omega^-$  hyperons in  $Z^0$  decays", P. Niss et al., DELPHI note 95-45  
PHYS 486.
- [8] DELPHI Collaboration, W. Adam et al., Z. Phys. **C70** (1996) 371.
- [9] "Strange Baryon Production in Hadronic Decays of the  $Z^0$ ", Peter Niss, Ph.D. thesis,  
University of Stockholm, 1996.
- [10] DELPHI Collaboration, W. Adam et al., Z. Phys. **C73** (1996) 11.
- [11] Yu.L. Dokshitzer, V.A. Khoze and S.I. Troyan, Z. Phys. **C55** (1992) 107.
- [12] ALEPH Collaboration, D.Buskulic et al., Phys.Lett. **B313** (1993) 535.
- [13] G. Borisov and C. Mariotti, Nucl. Instr. and Meth. **A372** (1996) 181.
- [14] ALEPH Collaboration, paper eps0419 contributed to the International Europhysics  
Conference on High Energy Physics, Brussels, Belgium, July 1995.
- [15] OPAL Collaboration, P.D. Acton et al., Z.Phys. **C73** (1997) 569.

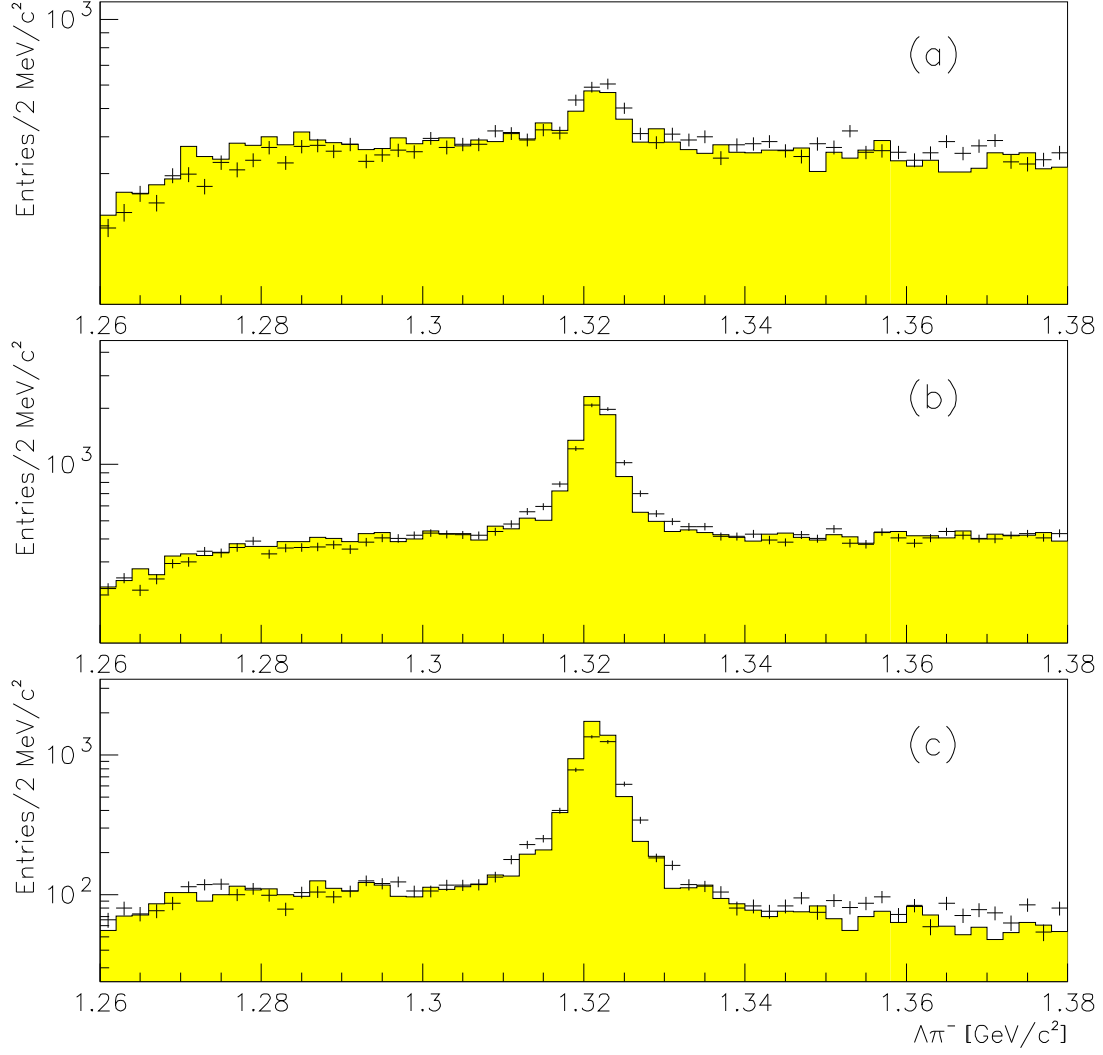


Figure 1: The  $\Xi$  ( $\Xi^-$  and  $\Xi^+$  added) signals in different chi-squared probability bins for data and simulation. Data are represented by the points with error bars and the simulation by the histograms. The histograms are normalized by the number of entries. **(a)** shows the  $\Xi$  signal without any cuts applied and having a chi-squared probability of less than 1 %. **(b)** shows the  $\Xi$  signal without any cuts applied and having a chi-squared probability greater than 1 %. **(c)** shows the  $\Xi$  signal after all cuts given in the text were applied and having a chi-squared probability greater than 1 %.

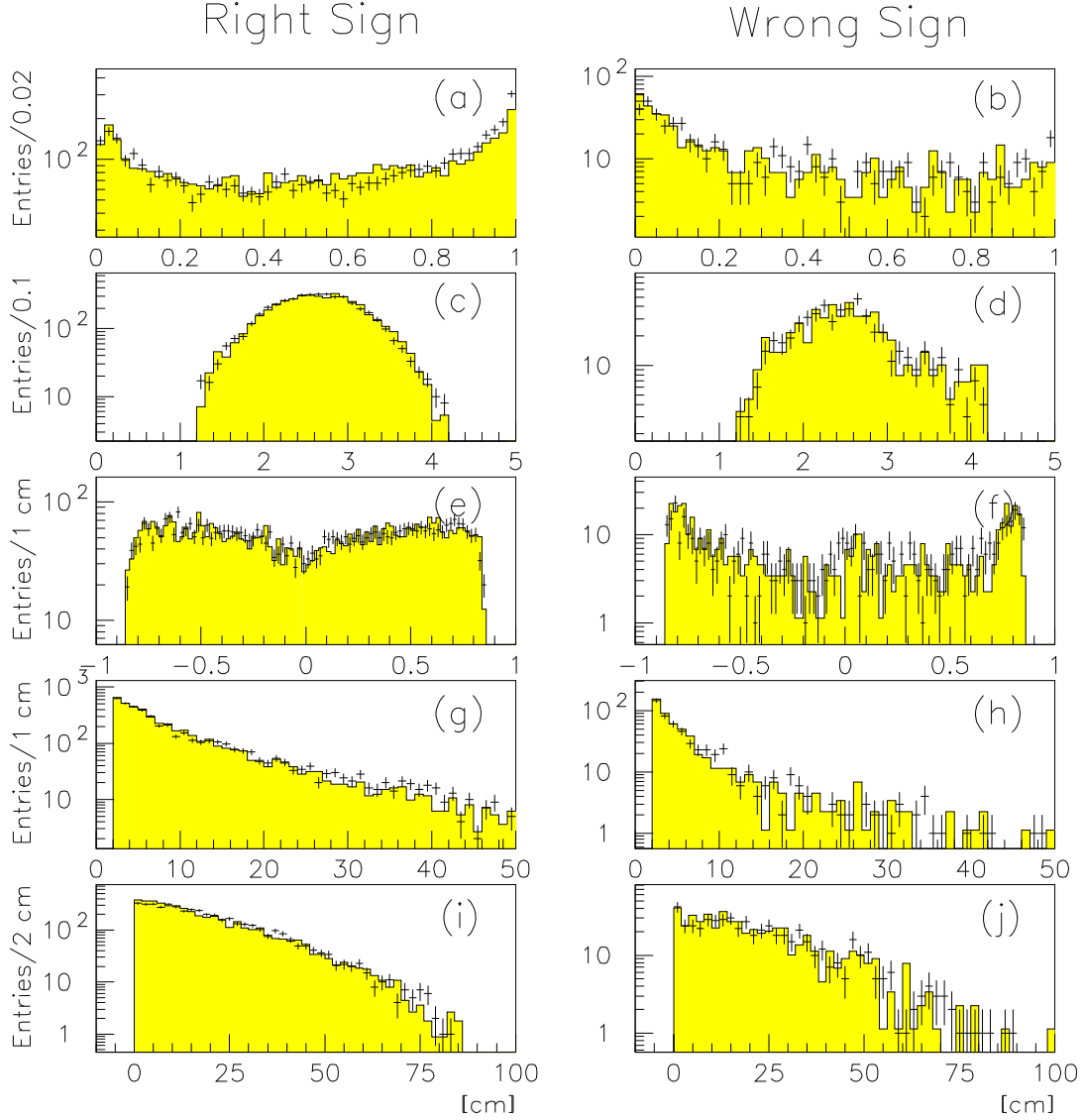


Figure 2: All variables used in the  $\Xi$  selection for candidates in the mass interval  $M_{\Xi} \pm 5 \text{ MeV}/c^2$ . The histograms are from the simulation and the points with error bars are the data. The years 1992 to 1995 have all been added, both for data and simulation. The simulation histograms are normalized to the data ones. All variables are shown as they are distributed after all cuts have been made.

- (a)–(b) Chi-squared probability.
- (c)–(d)  $\xi = -\ln(p_{\Xi}/p_{beam})$ .
- (e)–(f) Cosine of the polar angle  $\theta$  of the  $\Xi$  momentum.
- (g)–(h) Flight distance of the  $\Xi$  in the  $xy$  plane.
- (i)–(j) Distance in the  $xy$  plane between the  $\Lambda$  and  $\Xi$  decay points.

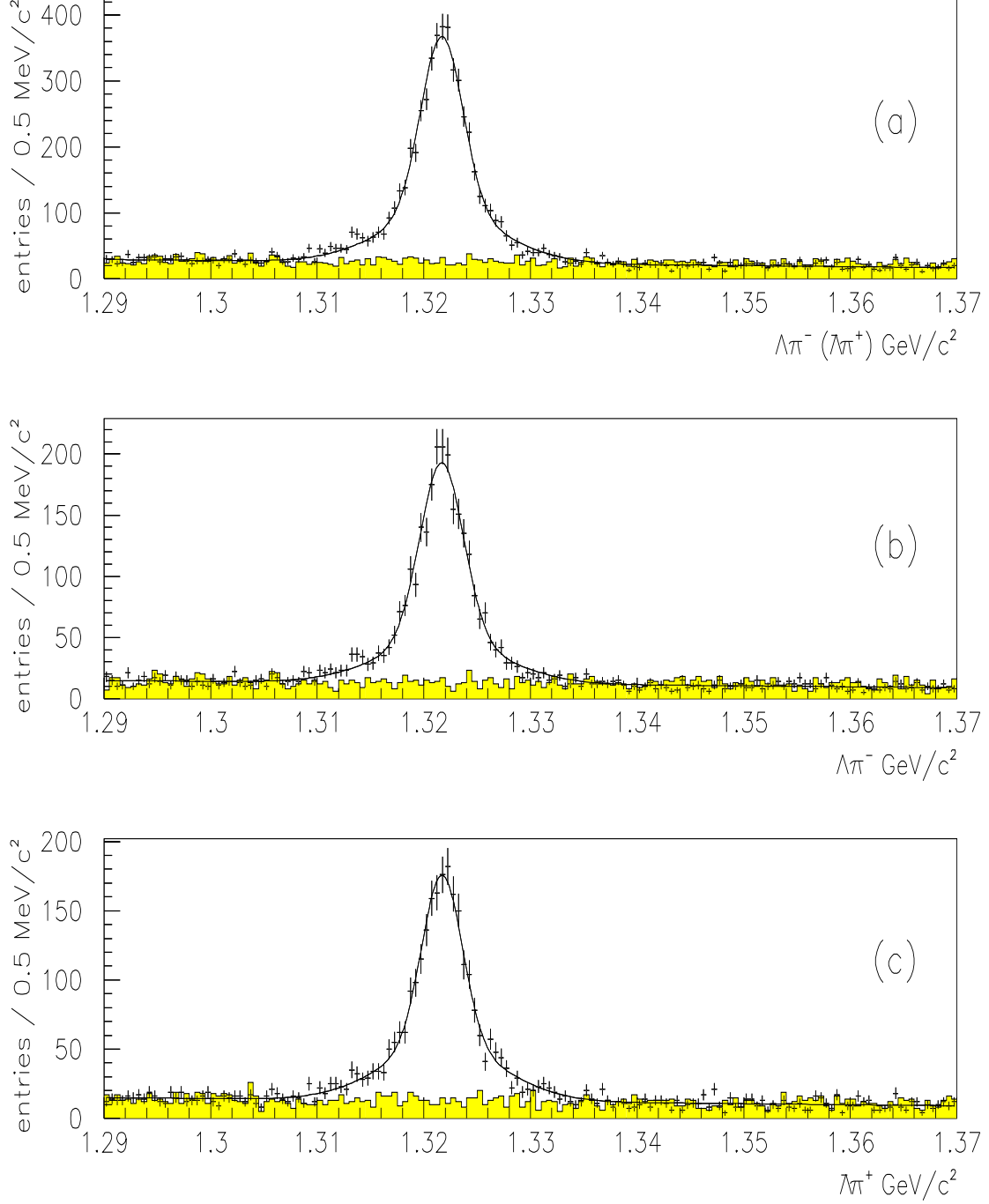


Figure 3: 1992-1995 data: **(a)**  $\Xi^-$  and  $\Xi^+$  sample. **(b)**  $\Xi^-$  sample. **(c)**  $\Xi^+$  sample. The data with error bars are the right sign ( $\Lambda\pi^-$ ,  $\bar{\Lambda}\pi^+$ ) combinations. The wrong sign ( $\Lambda\pi^+$ ,  $\bar{\Lambda}\pi^-$ ) combinations are shown as the solid line histograms. The  $\Xi$  signals are fitted to a sum of two Gaussian distributions as described in the text.



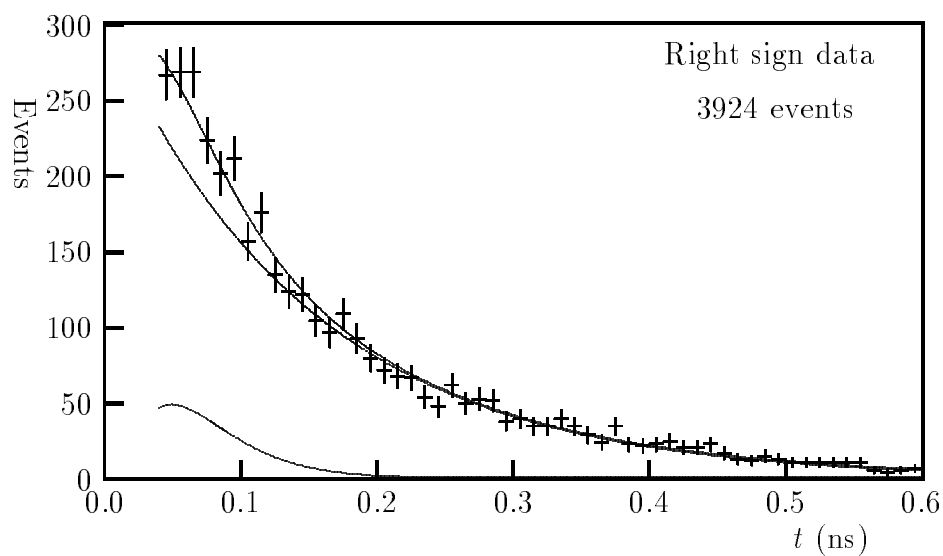


Figure 4: The observed time distribution in the right sign sample for 1992-1995 data. The lowest curve is the estimate of the contribution from combinatorial background events. These are assumed to be adequately described by the wrong sign combinations, as described in the text. The middle curve is the estimate of the proper  $\Xi^-$  and  $\Xi^+$  decays. The upper curve represents the fit to the observed time distribution, *i.e.* the sum of the two lower distributions.

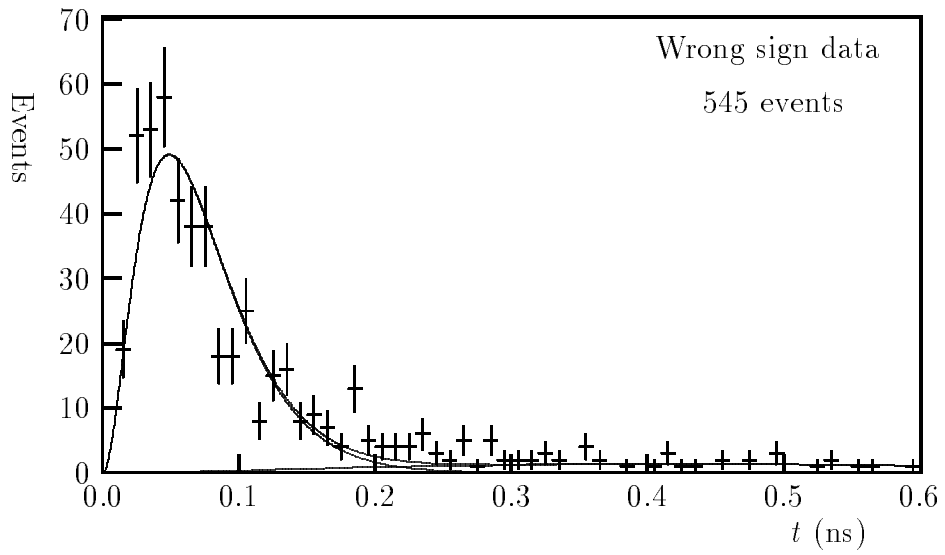


Figure 5: The observed time distribution in the wrong sign sample for 1992-1995 data. The two curves are the  $b$ -functions described in the text. The sum of them used to describe the combinatorial background is also shown. Only events with times larger than 0.04 ns were used in the fit.

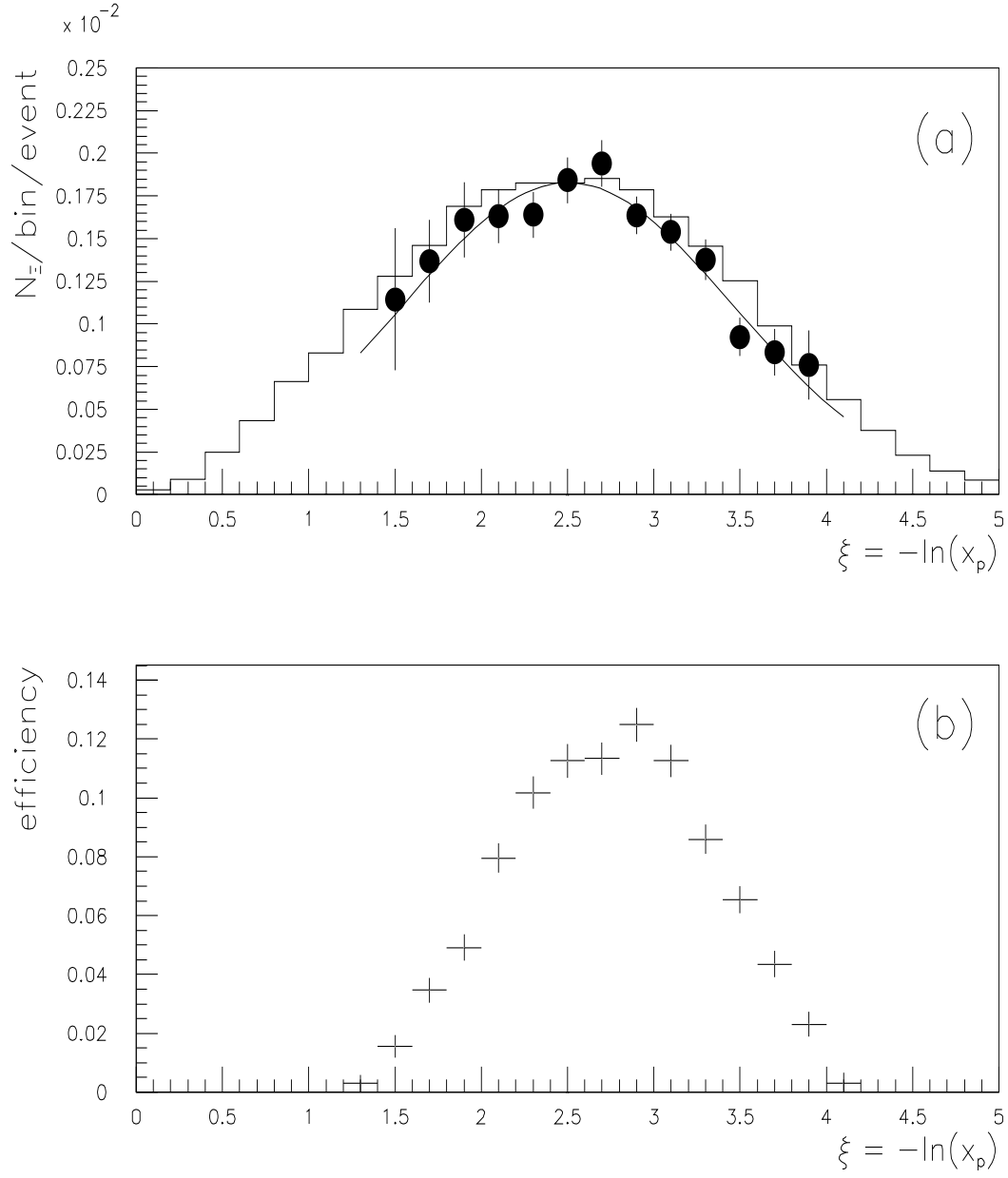


Figure 6: 1992-1995 data: **(a)** Efficiency corrected distribution of  $\xi = -\ln x_p$ : the points with error bars represent the measured  $\xi$  distribution, a fit to a Gaussian function is superimposed, and the JETSET  $\xi$  spectrum is shown as the solid histogram. **(b)** The  $\Xi^-$  reconstruction efficiency as a function of  $\xi$ .